Swiss J Geosci (2011) 104:67–79
DOI 10.1007/s00015-010-0048-7

Discovery of Ordovician–Silurian metamorphic monazite in garnet metapelites of the Alpine External Aiguilles Rouges Massif

Bernhard Schulz · Jürgen F. von Raumer

Received: 11 March 2010 / Accepted: 17 November 2010 / Published online: 15 February 2011

Abstract The pre-Mesozoic, mainly Variscan metamorphic basement of the Col de Bérard area (Aiguilles Rouges Massif, External domain) consists of paragneisses and micaschists together with various orthogneisses and metabasites. Monazite in metapelites was analysed by the electron microprobe (EMPA-CHIME) age dating method. The monazites in garnet micaschists are dominantly of Variscan age (330–300 Ma). Garnet in these rocks displays well developed growth zonations in Fe–Mg–Ca–Mn and crystallized at maximal temperatures of 670°C/7 kbar to the west and 600°C/7–8 kbar to the east. In consequence the monazite is interpreted to date a slightly pressure-dominated Variscan amphibolite-facies evolution. In mylonitic garnet gneisses, large metamorphic monazite grains of Ordovician–Silurian (~440 Ma) age but also small monazite grains of Variscan (~300 Ma) age were discovered. Garnets in the mylonitic garnet gneisses display high-temperature homogenized Mg-rich profiles in their cores and crystallized near to ~800°C/6 kbar. The Ordovician–Silurian-age monazites can be assigned to a pre-Variscan high-temperature event recorded by the homogenised garnets. These monazite age data confirm Ordovician–Silurian and Devonian–Carboniferous metamorphic cycles which were already reported from other Alpine domains and further regions in the internal Variscides.

Editorial handling: U. Schaltegger and E. Gnos.

B. Schulz (✉)
TU Bergakademie Freiberg, Institute of Mineralogy,
Brennhausgasse 14, 09596 Freiberg, Germany
e-mail: Bernhard.Schulz@mineral.tu-freiberg.de

J. F. von Raumer
Department of Geosciences, Université de Fribourg,
Chemin du Musée 6, 1700 Fribourg, Switzerland

Keywords Ordovician · Variscan · External Massiv · Garnet metapelites · EMP monazite age dating · P–T path · Polyphase metamorphism

1 Introduction

The Aiguilles Rouges Massif, one of the Alpine External Massifs, is relatively well preserved from Alpine overprint, attaining only the lowest greenschist facies grade with formation of stilpnomelane (von Raumer 1969). The pre-Mesozoic metamorphic basement served as example to discuss its derivation from the Early Palaeozoic Gondwana margin (von Raumer 1998, von Raumer and Neubauer 1993, von Raumer et al. 2002, 2003). During the earliest long-lasting evolution, since the Ediacarian to the Ordovician, continental extension and an Ordovician active margin setting predominated in this area (Stampfli et al. 2002). Apart from reduced sediments, a variety of acid and mafic magmatic rocks was generated in this period. During Variscan subduction and nappe stacking, these series became transformed into high-grade metamorphic rocks (metapelites and metagreywackes, diopside-marbles, orthogneisses, garnet-amphibolites), migmatites and rocks like eclogites, meta-ultrabasites and granulites. The dating on zircon and monazite had given mainly Carboniferous (~330–320 Ma) ages (Bussy and von Raumer 1994; von Raumer et al. 1996, 1999; Bussy et al. 2000; von Raumer and Bussy 2004). Since the findings of Paquette et al. (1989) also Early Palaeozoic protolith ages of magmatic rocks came into discussion (von Raumer et al. 2009).

As a considerable part of the Aiguilles Rouges metamorphic sequence is composed of metapelites and paragneisses, the presence of chemically zoned garnet together with adequate low-variance mineral assemblages

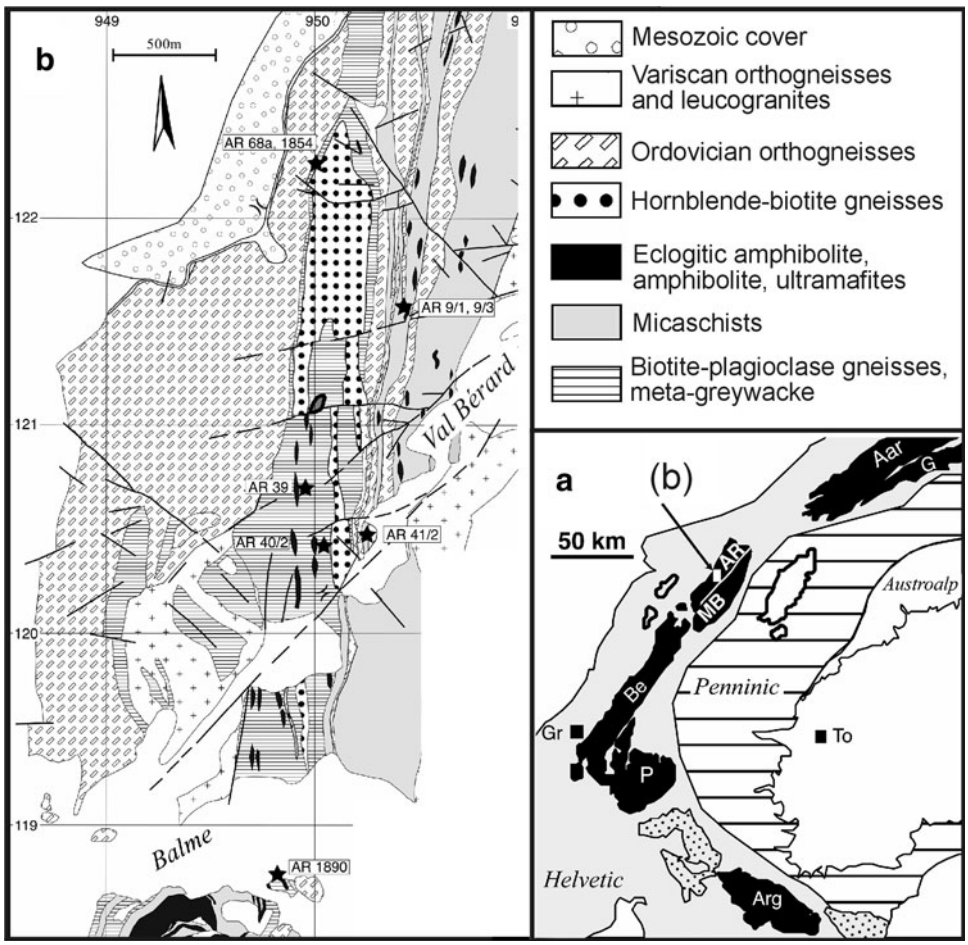

Fig. 1 **a** Position of the studied area within the pre-Alpine basement units of the Western Alps. External Massifs (*in black*) with the Aiguilles Rouges Massif (AR) and location of geological map in **b**. External massifs *Arg* Argentera, *Be* Belledonne, *G* Gotthard, *MB* Mont Blanc, *P* Pelvoux. Towns *Gr* Grenoble, *To* Torino. **b** Regional geological setting in the Col de Bérard region, petrographic map and sample locations. Geographic coordinates of the samples AR-9, 555440/94670; AR-39, 554900/93700; AR-40, 554940/93680; AR-41, 555200/93690; AR-68a, AR-1854, 555070/95470; AR-1890, 554800/91750 (Swiss Grid)

allowed to reconstruct the pressure–temperature (P–T)-evolution in some detail (Schulz and von Raumer 1993; Dobmeier 1998). A local Variscan migmatisation at ~650°C/<4 kbar has been described (Genier et al. 2008). The occurrence of monazite as an abundant accessory mineral in micaschists and paragneisses (Spear and Pyle 2002) provides an interesting opportunity for the dating of multiple thermal events (Finger et al. 2002; Fitzsimons et al. 2005; Pyle et al. 2005; Finger and Krenn 2007; Krenn and Finger 2007). In the present study, electron-microprobe dating of metamorphic monazite resulted in two distinct groups of ages. These age groups are related to different metamorphic events which were recorded by metapelitic assemblages with growth-zoned and high-temperature homogenised garnet. In this combination a yet merely presumed Early-Palaeozoic metamorphic event could be constrained in this part of the Variscan internal zone.

2 Sample description

Typical pre-Mesozic basement is observed between the Lac Cornu and Col de Bérard regions (Fig. 1). As the selected garnet-bearing metapelitic samples, already presented by Schulz and von Raumer (1993) turned out to bear monazite, they were re-investigated. In detail, garnet gneisses with a fine-grained foliated matrix surrounding lens-like microlithons up to 2 cm in length with large broken garnet porphyroblasts (up to 1.5 cm in diameter) occur at a new location AR-1890 and at AR-40 (sample E in Schulz and von Raumer 1993). Detailed mapping revealed that both samples belong to the same lithological horizon with variable thickness between 1 and 30 m, which can be traced over several hundred meters. Due to the comparably fine-grained foliated matrix contrasting the large garnet porphyroblasts, this horizon resembles a high temperature mylonite and is labelled as a mylonitic garnet gneiss.

The samples AR-68a and AR-1854 (samples C and D in Schulz and von Raumer 1993) are micaschists from a western series (Fig. 1b). Both samples are from a distinct small horizon near to layers of amphibolite. They contain large euhedral garnet porphyroblasts up to 1.5 cm in diameter which enclose biotite, muscovite, plagioclase and quartz. A main foliation labelled S_2 is underlined by coarse-grained mica. Sample AR-68a has kyanite enclosed

in plagioclase, fibrolitic sillimanite with biotite in S_2 and large post-S_2 aggregates of andalusite, but no staurolite. Sample AR-1854 bears also these aluminosilicates but has staurolite which is enclosed in garnet. The samples AR-41 and AR-9 are garnet micaschist and correspond to the samples A and B in Schulz and von Raumer (1993). They belong to the eastern part of the sequence (Fig. 1b). The garnets contain inclusions of mica, plagioclase and quartz in planar or strongly curved trails S_1i indicating a syntectonic crystallization of the porphyroblasts. The garnet porphyroblasts occur in microlithons with elongated plagioclase and quartz and are surrounded by an anastomosing main foliation S_2 underlined by mica. Staurolite is not enclosed in garnet. Kyanite occurs in distinct porphyroblasts. In some S_2 layers biotite is strongly altered and replaced by fibrolitic sillimanite.

3 Analytical methods

Quantitative analyses of garnet porphyroblasts and coexisting biotite and plagioclase, enclosed in garnet or within microstructural domains, were performed with an electron microprobe JEOL JXA8900 RL at the Institut für Werkstoffwissenschaft at Freiberg/Saxony. The electron beam was set at 20 kV/20 nA and the common matrix ZAF corrections were applied. Garnet and plagioclase were analysed along transgranular profiles. Biotite was characterized by analyses from cores and rims (Schulz and von Raumer 1993).

Analysis of Th, U and Pb for calculation of monazite model ages, as well as for Ca, Si, LREE and Y for corrections and evaluation of the mineral chemistry were carried out on a JEOL JXA 8200 at the Chair of Mineralogy, University of Erlangen-Nürnberg (Schulz et al. 2007). The Mα1 lines of Th and Pb and the Mβ1 lines for U of a PETH crystal were selected for analysis. Resulting absolute errors (2σ) at 20 kV acceleration voltage, 100 nA beam current, 5 µm beam diameter and counting times of 320 s (Pb), 50 s (U) and 40 s (Th) are typically 0.008–0.012 wt% for Pb, 0.020–0.025 wt% for U and 0.02–0.03 wt% for Th. The lines Lα1 for La, Y, Ce; Lβ1 for Pr, Sm, Nd, Gd and Kα1 for P, Si and Ca were chosen. Orthophosphates of the Smithsonian Institution were used as standards for REE analysis (Jarosewich and Boatner 1991; Donovan et al. 2003). Calibration of PbO was carried out on a vanadinite standard. The U was calibrated on an appropriate glass standard with 5 wt% UO_2. The age of the *Madmon* monazite (Schulz et al. 2007), dated by SHRIMP at 496 ± 9 Ma and numerous Pb–Pb–TIMS monazite evaporation data (K. Bombach, Freiberg, unpublished analytical method) at 497 ± 2 Ma, was also determined at 503 Ma by the EMP monazite dating routines established at facilities in Salzburg and BRGM Orléans (Finger and Helmy 1998; Cocherie et al. 1998). The *Madmon* contains ThO_2 at around 10 wt%, as determined by LA-ICPMS and by the microprobe at University of Salzburg. *Madmon* was used for calibration and offline re-calibration of ThO_2 as well as for the control of data. Interference of YLγ on the PbMα line was corrected by linear extrapolation as proposed by Montel et al. (1996). An interference of ThMγ on UMβ was also corrected by using a Th-glass standard. Interference of a Gd-line on UMβ needs correction when Gd_2O_3 in monazite is >5 wt%. These parameters matched the analytical problems discussed in Willams et al. (2006) in the best way. Representative data are given in Table 1.

4 Monazite ages and mineral chemistry

The EMP monazite dating revealed two distinct generations of ages in the mylonitic garnet gneisses AR-1890 and AR-40. An older group of ages around 440 Ma (Late Ordovician to Early Silurian) has been found in large matrix monazite grains next to the garnet porphyroblasts (Fig. 2a) or in monazites enclosed in the garnets (Fig. 2b). The monazites enclosed in garnet exclusively display the Ordovician–Silurian ages. In some of the larger matrix grains allowing several analyses, some marginal analytical points yielded also Carboniferous ages (Fig. 2c, e). Furthermore the Carboniferous (labelled as Variscan) ages occur exclusively in multigrain aggregates of monazites with grain sizes <20 microns, aligned along the mylonitic foliation. In some cases these small monazites appear as satellites around apatite (Fig. 2d). In the ThO_2* versus PbO diagram (Suzuki et al. 1994), the Ordovician–Silurian and Variscan monazite ages appear along two distinct isochrons (forced through zero, Montel et al. 1996). Although the data scatter somewhat around the isochrons, there are no monazite analyses with intermediate ages in between these groups (Fig. 3a, b). The Ordovician–Silurian monazites in matrix and enclosed in garnet have much higher Y_2O_3 (~3.2 wt%), whereas the maximal Y_2O_3 in the Variscan monazites are only 1.5 wt% (Fig. 4a). Both age groups of monazites have similar contents of LREE, ThO_2 and UO_2 (Fig. 4c, e; Table 1).

Variscan age monazites dominate in the micaschist samples. Only a few single analyses in the cores of the matrix grains with sizes of 10–40 µm provided the Ordovician–Silurian ages and are interpreted as metamorphic relics (sample AR-41). The Variscan ages occur in large monazites which are elongated along the foliation planes (Fig. 2). Monazites enclosed in garnet are also of Variscan age, but appear as slightly older (~330 Ma, sample AR-41) than monazites (~312 Ma) in the matrix (Figs. 2g-i, 3d, e). In sample AR-1854 the largest variation of 0.01–2.7 wt% Y_2O_3 can be observed. However, in one sample (AR-68a), monazite comparably rich in Y_2O_3

Table 1 Electron microprobe analyses of metamorphic monazite from mylonitic garnet gneisses and micaschists of the Col de Bérard region in the Aiguilles Rouges Massif

Monazite		SiO_2	P_2O_5	CaO	Y_2O_3	La_2O_3	Ce_2O_3	Pr_2O_3	Sm_2O_3	Nd_2O_3	Gd_2O_3	ThO_2	UO_2	PbO	Total	Th	U	Pb	Th*	Age (Ma)
AR-1890-Mnz2	79	0.14	30.33	1.18	2.16	13.56	27.52	3.07	1.80	12.43	1.49	5.06	0.43	0.122	99.29	4.45	0.38	0.113	5.68	446 ± 47
AR-1890-Mnz2	83	0.08	30.36	0.98	2.48	13.35	27.71	3.07	2.06	12.88	1.46	3.33	1.13	0.131	99.01	2.93	0.99	0.122	6.18	442 ± 44
AR-1890-Mnz2	86	0.08	29.92	1.12	2.41	12.95	27.25	3.08	2.04	12.71	1.60	3.85	1.35	0.158	98.51	3.39	1.19	0.147	7.29	451 ± 37
AR-1890-Mnz1	6	0.11	30.21	1.10	3.30	13.03	26.96	3.05	2.30	12.63	1.72	4.39	0.64	0.121	99.55	3.86	0.57	0.112	5.71	440 ± 47
AR-1890-Mnz1	14	0.77	30.14	1.14	0.92	13.61	28.31	3.18	2.51	14.24	1.94	2.15	0.84	0.060	99.79	1.89	0.74	0.056	4.28	295 ± 63
AR-1890-MAg2	18	0.56	29.13	0.90	1.10	14.27	27.72	3.24	2.15	12.96	1.49	3.11	0.60	0.065	97.30	2.73	0.53	0.060	4.46	302 ± 60
AR-1890-MAg2	22	0.60	30.34	1.14	1.37	13.87	28.02	3.14	2.21	12.85	1.67	4.74	0.52	0.084	100.54	4.17	0.45	0.078	5.64	310 ± 48
AR-40-Mnz2	147	0.06	30.33	1.10	0.81	12.46	27.68	3.22	2.68	14.08	1.85	4.67	0.37	0.110	99.39	4.10	0.32	0.102	5.16	442 ± 52
AR-40-Mnz2	150	1.34	29.33	1.08	2.21	10.92	24.85	3.07	2.68	13.69	2.32	4.82	0.25	0.106	96.67	4.24	0.22	0.098	4.96	442 ± 54
AR-40-MiGrt1	158	0.08	30.55	1.05	2.96	13.35	27.67	2.98	1.74	12.30	1.52	4.17	0.69	0.119	99.18	3.67	0.61	0.110	5.67	435 ± 47
AR-40-MiGrt1	162	0.11	30.51	1.10	2.80	13.25	27.34	2.98	1.54	12.34	1.50	4.31	0.76	0.130	98.66	3.78	0.67	0.121	5.99	450 ± 45
AR-40-MiGrt1	173	0.12	30.07	0.99	1.25	13.12	28.38	3.25	1.91	13.83	1.63	4.53	0.29	0.103	99.46	3.98	0.25	0.095	4.81	443 ± 56
AR-40-Mnz7	181	0.36	29.78	1.06	1.51	13.06	27.19	3.03	2.37	12.75	1.98	5.47	0.31	0.083	98.96	4.80	0.28	0.077	5.70	303 ± 47
AR-41-MiGrt14	99	0.28	30.29	0.99	0.11	14.92	30.11	2.97	1.35	12.26	1.16	5.20	0.47	0.094	100.20	4.57	0.41	0.087	5.90	331 ± 38
AR-41-MiGrt18	111	0.27	30.23	0.91	0.07	14.91	30.11	2.99	1.45	12.58	0.98	4.91	0.30	0.080	99.78	4.32	0.26	0.074	5.17	320 ± 43
AR-41-MiGrt18	112	0.26	29.42	0.87	0.10	14.82	29.68	2.95	1.61	12.14	1.10	4.50	0.31	0.078	97.84	3.96	0.27	0.073	4.84	336 ± 46
AR-41-MiGrt18	113	0.32	30.11	0.93	0.10	14.49	29.73	2.92	1.63	12.61	1.41	5.10	0.36	0.090	99.80	4.48	0.31	0.084	5.50	340 ± 41
AR-41-MiGrt18	114	0.23	30.36	0.80	0.08	15.09	30.67	3.14	1.66	12.63	1.03	4.23	0.29	0.071	100.26	3.72	0.26	0.066	4.55	323 ± 49
AR-41-MiGrt19	115	0.41	30.02	0.98	0.07	14.56	29.39	2.96	1.90	12.43	1.50	5.67	0.36	0.096	100.34	4.98	0.31	0.089	6.00	333 ± 37
AR-41-MiGrt19	116	0.23	30.36	0.72	0.08	15.08	30.94	3.06	1.70	12.91	1.32	3.80	0.30	0.067	100.56	3.34	0.26	0.062	4.20	330 ± 53
AR-1854-Mnz5	38	0.30	29.77	1.14	1.52	13.19	27.51	3.02	2.42	12.97	1.61	5.08	1.00	0.108	99.63	4.46	0.88	0.100	7.31	307 ± 31
AR-1854-MiGrt5	54	1.58	28.58	1.60	0.06	12.61	27.30	2.65	1.88	11.62	0.94	11.58	0.31	0.163	100.87	10.18	0.28	0.151	11.07	305 ± 20
AR-1854-MiGrt10	63	3.83	26.85	1.56	0.07	12.37	26.14	2.43	1.35	10.47	0.91	11.23	0.32	0.163	97.71	9.86	0.28	0.152	10.79	314 ± 21
AR-9-Mnz3	27	0.37	29.70	1.19	1.50	13.96	26.87	2.92	2.23	12.68	1.84	6.22	0.38	0.101	99.93	5.46	0.33	0.094	6.54	321 ± 34
AR-9-Mnz14	68	0.25	29.63	1.43	0.82	13.27	27.43	3.01	2.20	12.71	1.62	6.96	0.58	0.118	100.02	6.11	0.51	0.109	7.77	316 ± 29
AR-9-Mnz16	50	0.29	30.03	1.12	0.61	13.87	27.63	3.05	1.93	12.46	1.54	5.79	0.37	0.093	98.76	5.09	0.33	0.086	6.14	314 ± 36
AR-68a-Mnz2	14	0.35	30.18	1.62	1.68	12.00	26.42	2.84	2.24	11.79	1.76	7.38	1.44	0.150	99.84	6.49	1.27	0.140	10.59	296 ± 21
AR-68a-Mnz2	18	0.29	30.37	1.19	1.43	12.74	27.81	3.00	2.33	12.14	1.74	5.36	1.09	0.111	99.59	4.71	0.96	0.103	7.81	296 ± 29
AR-68a-Mnz5	41	0.48	30.59	1.31	1.23	12.55	27.63	2.87	2.29	12.20	1.63	6.18	1.00	0.126	100.09	5.43	0.88	0.117	8.29	317 ± 27
Madmon-ave50		2.80	25.74	0.14	0.99	7.69	25.14	3.70	4.51	15.61	4.51	10.67	0.41	0.256	100.04	9.38	0.36	0.238	10.56	502 ± 11

Th* is calculated from Th and U after Suzuki et al. (1994). Monazite ages from single analyses are given with 2sigma error (see text). Mnz monazite single grain; MAg satellite small monazite grains; MiGrt monazite grains enclosed in garnet. Data from reference standard monazite Madmon (Schulz et al. 2007) is mean of 50 single analyses performed during sessions on the Aiguilles Rouges samples

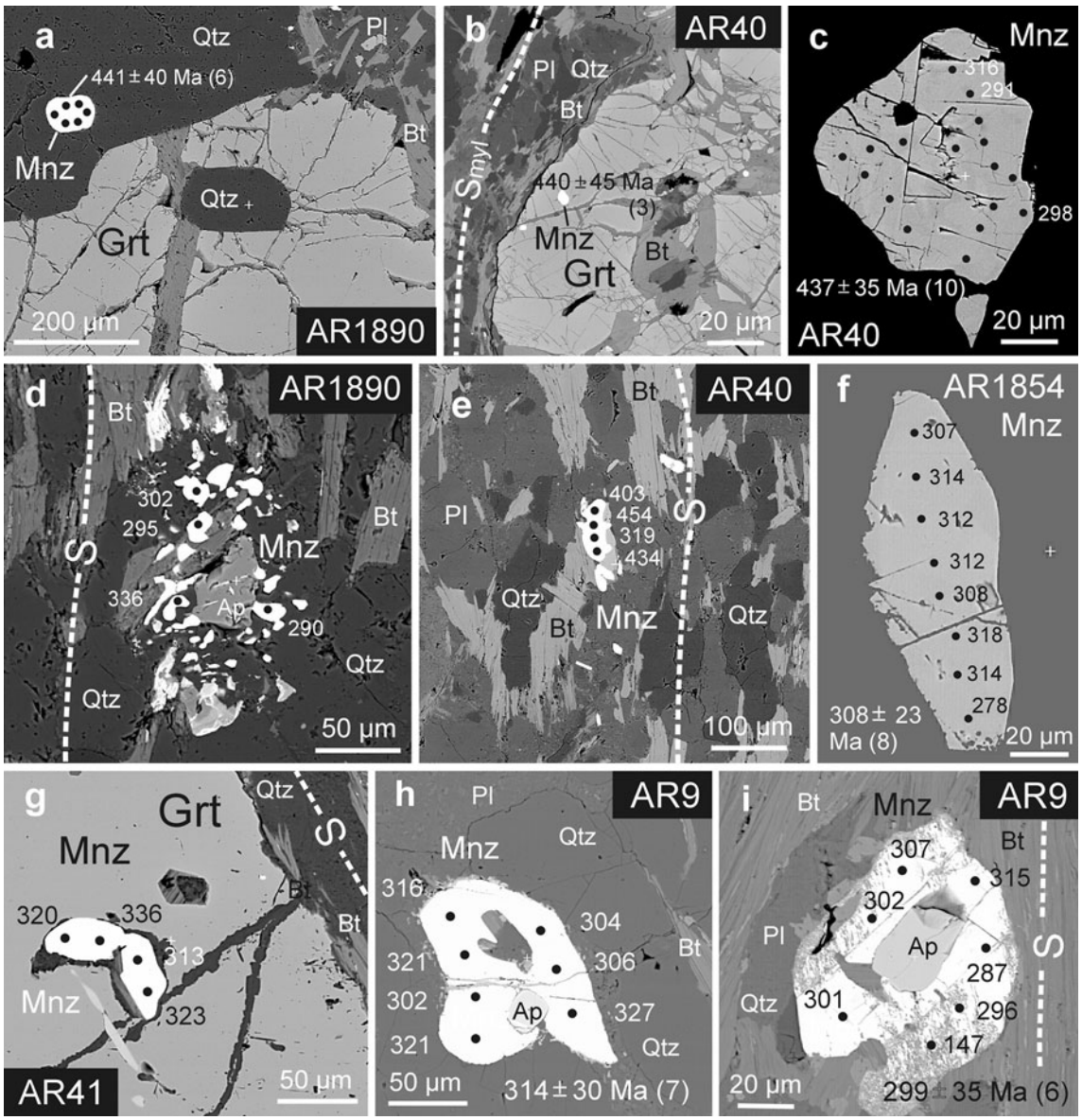

Fig. 2 Backscattered electron images (BSE) of monazite in mylonitic garnet gneisses and garnet-bearing micaschists. Numbers are EMP chemical ages from monazite, calculated as weighted means with 2 sigma error (see text) or from single analyses. Locations of microprobe analyses are marked. **a** Large Ordovician monazite grain in low-strain domain near large garnet porphyroblast in mylonitic garnet gneiss. **b** Large Ordovician monazite enclosed in garnet porphyroblast in mylonitic garnet gneiss. **c** Large monazite grain in mylonitic garnet gneiss. Some analyses with Variscan ages reveal partial recrystallization of the monazite. **d** Reaction site in mylonitic garnet gneiss with Variscan monazite satellites around central apatite. **e** Ordovician monazite in mylonitic high strain domain in garnet gneiss. **f** Homogeneous Variscan monazite elongated parallel to the foliation in a micaschist. **g** Variscan monazite enclosed in micaschist garnet. Monazite may have crystallized along cracks subsequent to garnet. **h** Homogeneous Variscan monazite with enclosed apatite. **i** Variscan monazite with partial decomposition along the margin. Decomposed parts give random post-Variscan ages

(1.0–2.5 wt%) is dominant. Quite limited variations occur in samples AR-9 (Y_2O_3 0.5–1.5 wt%) and in sample AR-41, where all monazites are very low in Y_2O_3 (0.01–0.2 wt%, Fig. 4b). The ThO_2 of the Variscan monazites in the micaschists display a similar variation from 2 to 7 wt% as in the mylonitic garnet gneisses, however the sample AR-1854 is an exception with a wide range of 2–12 wt% ThO_2 (Fig. 4e, f).

5 Garnet mineral chemistry and geothermobarometry

Mineral-chemical data from the samples AR-40, AR-68a, AR-1854, AR-9, AR-41 and also from an eclogitic amphibolite (Sample AR-39, or sample F, respectively) is reported in detail in Schulz and von Raumer (1993). For the study presented here, the data were completed by analyses of garnets and related phases in the mylonitic

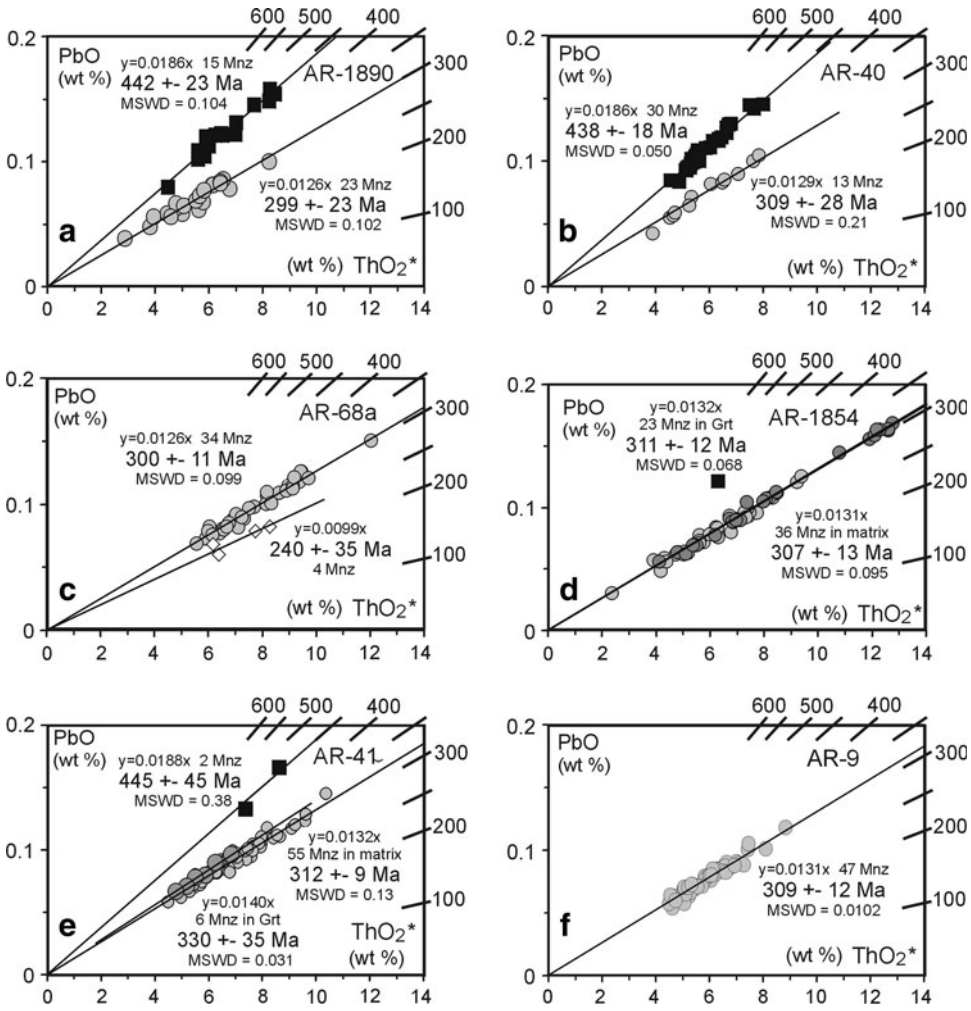

Fig. 3 Th–U–Pb CHIME model ages of monazite in the Col de Bérard region of the Aiguilles Rouges Massif. Total PbO versus ThO_2* (wt%) isochron diagrams; ThO_2* is $ThO_2 + UO_2$ equivalents expressed as ThO_2, after Suzuki et al. (1994). Isochrons are calculated from regression forced through zero as proposedby Montel et al. (1996). Isochron ages match weighted average ages with error calculated according to Ludwig (2001). The MSWD values refer to 95% confidence interval. Age bars are given in Ma. **a**, **b** Mylonitic garnet gneisses with Ordovician and Variscan (Carboniferous) monazite ages. **c**–**f** Variscan (Carboniferous) monazites in garnet-bearing micaschists. Pre- and post-Variscan monazite ages and data from monazite enclosed in garnet are marked

garnet gneiss sample AR-1890. In the mylonitic garnet gneisses the compositional profiles are flat in the cores with up to 30% pyrope and low spessartine and grossular (<2%) contents. Toward the rims a decrease of pyrope and increase of grossular is observed (Fig. 5a). Such garnet zonation profiles are typical of homogenisation of the cores by diffusion at high temperatures and resorption of the rims during retrogression (Spear 1993). Biotite along the mylonitic foliation has *X*Mg of 0.46–0.51. Plagioclase in the matrix is zoned with anorthite contents of 22% in the cores and 33% in the rims, but poorly zoned porphyroblasts ($An_{26–29}$) are abundant.

The garnets in the micaschist samples (Fig. 5b, c) display growth zonations with considerable decrease of spessartine (Mn) contents from cores to rims while pyrope (Mg) increases. The spessartine contents in garnet cores are quite high (up to 20% in sample AR-41; between 5 and 10% in the other samples) and decrease toward the rims. The maximal pyrope contents in the garnet rims are 17%. Zonations are significant even in large garnet porphyroblasts up to 1.5 cm in diameter as in samples AR-68a and AR-1854. They reflect growth zonation trends during increasing temperatures as can be suggested from the increase of pyrope toward the rims. Semiquantitatively, increasing and decreasing pressure is indicated by the grossular zonations (Spear 1993).

The sample AR-39 is an eclogitic amphibolite lens within the western part of the sequence. A compositional layering is defined by green amphibole, garnet, clinopyroxene-plagioclase symplectites, plagioclase and quartz. The xenoblastic garnets (2–3 mm in diameter) enclose small clinopyroxene, plagioclase, quartz and opaques and are invaded by green amphibole. Matrix clinopyroxene occurs with plagioclase in coarse-grained symplectites. Green amphibole and quartz form a coarse-grained matrix. The garnets are only slightly zoned with 17–20 mol% pyrope, 23–26% grossular, 53–55% almandine and <2% spessartine. Clinopyroxene enclosed by the garnets is omphacitic ($Jd_{21–26}$). Jadeite contents of symplectitic clinopyroxenes are lower ($Jd_{9–15}$). Plagioclase is $An_{15–17}$ in all microstructural positions. Obviously the symplectitic

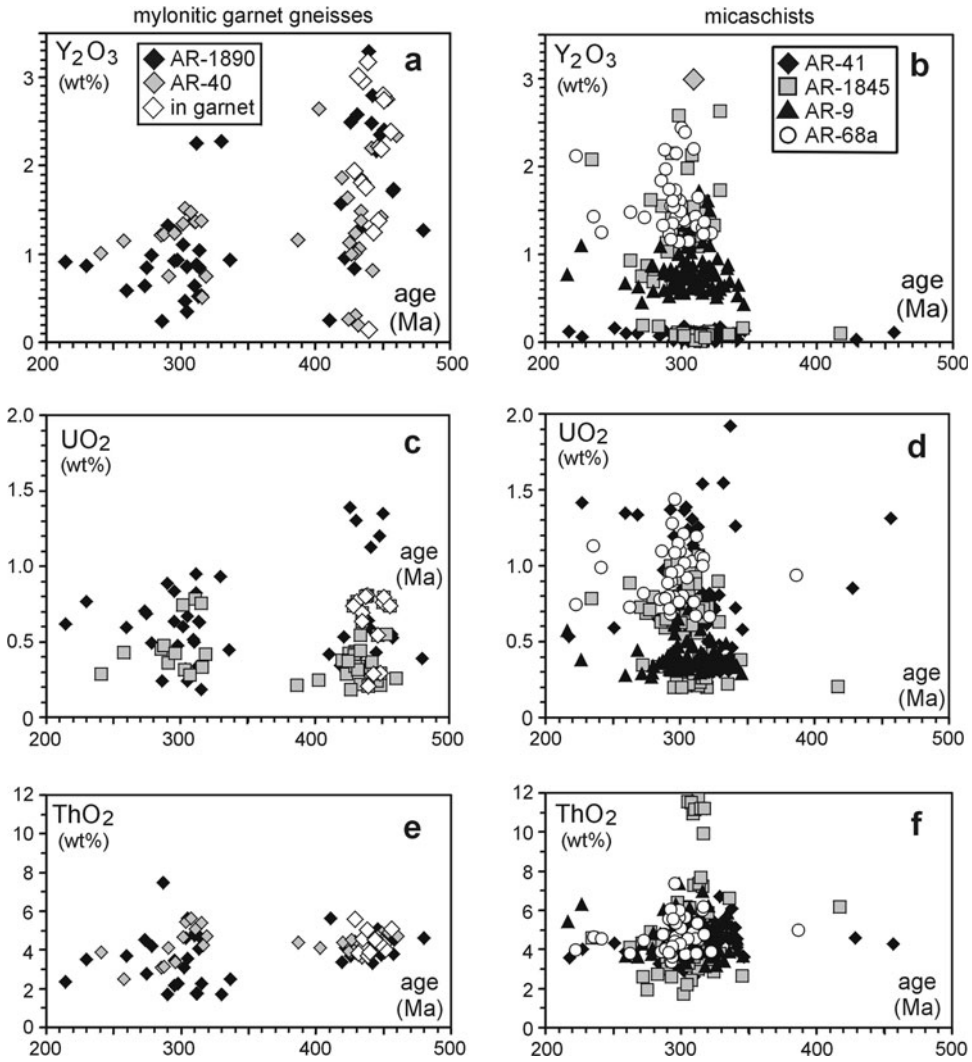

Fig. 4 Mineral chemistry of monazite versus Th–U–Pb chemical ages. **a**, **b** Y_2O_3 in monazite versus age in mylonitic garnet gneisses and in micaschists. **c**, **d** UO_2 contents in monazite versus age. **e**, **f** ThO_2 in monazite versus age. Legends in **a**, **b** apply for all parts

clinopyroxenes resulted from a breakdown of high-pressure-stage clinopyroxenes (up to Jd_{26}) which are still preserved in garnet inclusions.

In the mylonitic garnet gneisses the cores of homogenised garnets as well as their rims are interpreted to be in equilibrium with biotite and plagioclase cores and rims in the matrix. In the micaschist samples, the cores of zoned garnet and its plagioclase and biotite inclusions, as well as cores of zoned matrix plagioclase should have crystallised at early stages of the metamorphic evolution. A late stage of metamorphism is documented by garnet inner rims, large biotite which crystallised in the microlithons or in pressure shadows around the garnet porphyroblast, and the rims of zoned matrix plagioclase (Tracy 1982; St-Onge 1987; Triboulet and Audren 1985; Schulz 1993). P and T have been calculated from the mylonitic garnet gneisses and the garnet micaschists by the garnet-biotite thermometer of Bhattacharya et al. (1992) in combination with linearised calibration of the garnet-aluminosilicate-plagioclase (GASP) and the garnet-muscovite-biotite-plagioclase (GMBP) barometers, based on an internally consistent thermodynamic data set (Holland and Powell 1990), with the activity models for garnet given by Ganguly et al. (1996) and for plagioclase as proposed by Powell and Holland (1993). Tentative calculations by other calibrations (Holdaway 2001), as mentioned in Wu and Cheng (2006), yielded not substantially different results.

In detail, in the mylonitic garnet gneisses the thermobarometric calculations suggest that the Mg-rich homogenized garnet cores crystallized at high temperatures near to 800°C/6 kbar. From the zoned garnet rims it was possible to calculate 650°C/3 kbar (Fig. 6a). The P–T data from both analysed samples overlap within error. According to the garnet zonation trends (Fig. 5b, c), from samples AR-1854 and AR-68a maximal temperatures of 670°C/7 kbar have been calculated (Fig. 6b). The geothermobarometric re-calculations from garnet rims and inner parts in samples AR-9 and AR-41 yielded temperatures from 500 to 600°C between 11 and 6 kbar which are arranged along a prograde-retrograde P–T path along decreasing pressures (Fig. 6c).

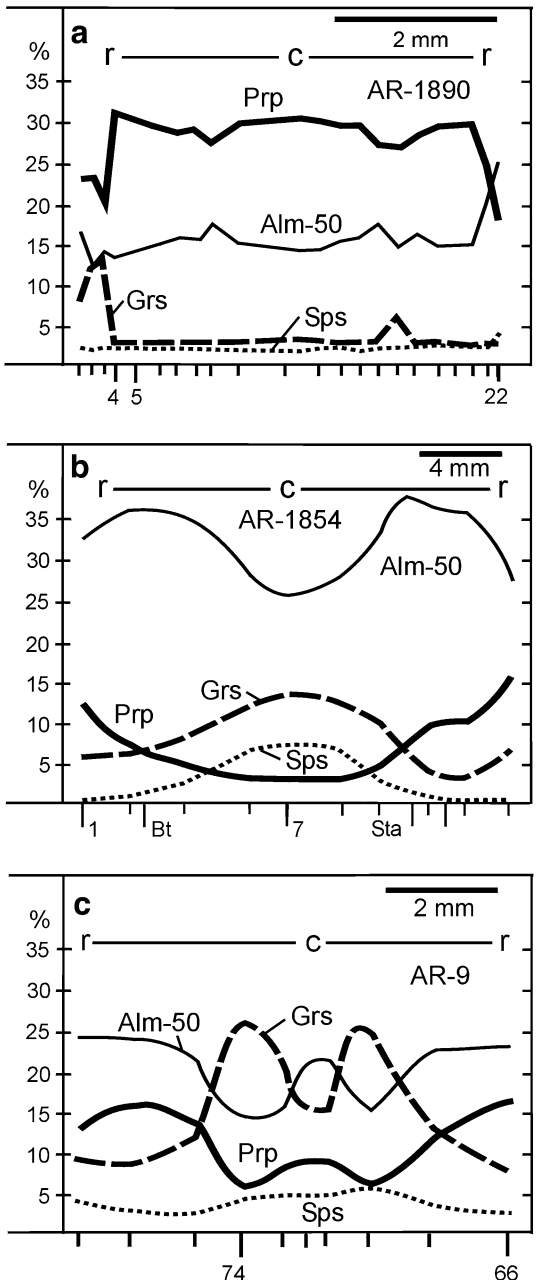

Fig. 5 **a–c** Garnet zonations in almandine (Alm-50, due to scale), grossular (Grs), pyrope (Prp) and spessartine (Sps) components. Single analyses used for pressure and temperature calculations in Fig. 6 are marked with numbers. Position of biotite (Bt) and staurolite (Sta) enclosed in garnet are marked. **a** Garnet in mylonitic garnet gneiss with homogeneous pyrope-rich cores and rims with lower Mg and variable grossular (Ca). **b**, **c** Growth-zoned garnets with spessartine-rich cores in micaschists

In the eclogitic amphibolite sample AR-39 the P–T estimates for crystallisation of garnet and enclosed clinopyroxenes center around 650°C/13 kbar (Fig. 6b) when various calibrations of the garnet-clinopyroxene-plagioclase geothermo-barometers (Ellis and Green 1979; Holland 1980; Newton and Perkins 1982; Krogh 1988; Perchuk 1991; Berman et al. 1995) are applied. A subsequent stage of the metamorphic evolution has been recorded by the tschermakitic hornblendes with rather homogeneous compositions. Application of an updated amphibole endmember geothermobarometer for assemblages with oligoclase (Zenk and Schulz 2004) yielded 630°C/6 kbar (Fig. 6b). P–T data from the eclogitic amphibolite and the micaschists from the western part of the series can be combined along a nearly isothermal decompression path with the maximum temperatures at ~670°C/7 kbar. This contrasts maximal temperatures around ~600°C/7–8 kbar along a decompression path in the micaschists to the east (Fig. 6d).

6 Discussion: an Ordovician–Silurian metamorphic event?

In micaschists and mylonitic garnet gneisses two age generations of metamorphic monazite are observed. The older age group of around 440 Ma (Ordovician–Silurian) occurs dominantly in the mylonitic garnet gneisses. A younger Variscan age group between 330 Ma (when enclosed in garnet) and 310–300 Ma is observed in all studied samples, but is dominant in the micaschists (Fig. 3). The Variscan EMP-CHIME Th–U–Pb monazite ages confirm the TIMS U–Pb monazite ages in micaschists (327 ± 2 Ma) and leucosomes (320 ± 1 Ma) from the Emosson area (Bussy et al. 2000) and the 337–316 Ma Ar–Ar white mica cooling ages in the western parts of the massif (Dobmeier 1998).

Geothermobarometry based on mineral zonations of garnet-bearing assemblages revealed a considerable range of maximal temperatures, which were passed in the course of prograde and retrograde P–T paths. Temperatures near to 800°C are calculated from garnets with homogenised core profiles in the mylonitic garnet gneisses and are considered as the possible upper limit. The growth-zoned garnets in the micaschists crystallized at lower maximal temperatures, at 670°C to the W and at 600°C to the E. These marked differences of maximal temperatures observed in samples situated in close distance led to a tectonic model of a telescoped Variscan metamorphic zonation (Schulz and von Raumer 1993). According to this model, Variscan metamorphic zones with different maximal temperatures, as observed from the western and eastern series of metapelites (Figs. 1b, 6b), were juxtaposed in a strike-slip deformational regime during the uplift.

These marked differences in maximal temperatures calculated from the garnet-bearing assemblages in the two rock types are reflected by the mineral chemistry of the monazites. In the mylonitic garnet gneisses the mole fraction of the xenotime component is higher (up to 0.08, X(Y + HREE) calculated as described in Pyle et al. 2001) in Ordovician–Silurian monazite compared to the Variscan

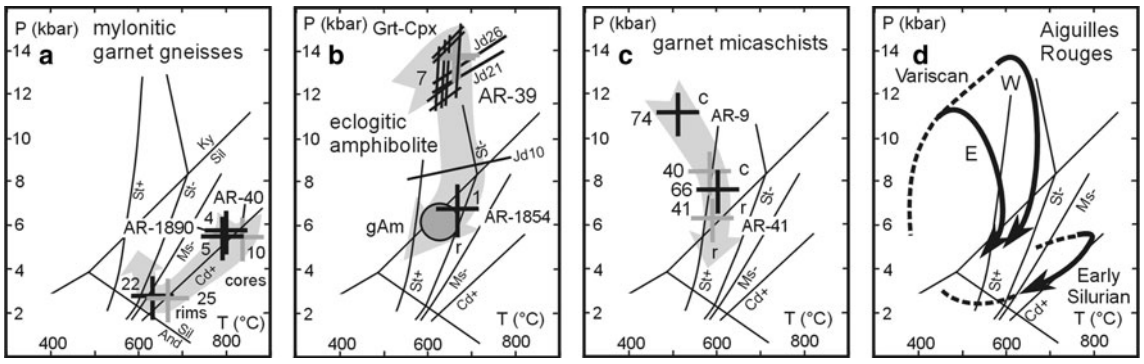

Fig. 6 P–T data and P–T path segments from mylonitic garnet gneisses, micaschists and eclogitic amphibolite of the Col de Bérard region. Large crosses represent P–T results from the Grt-Bt-thermometer of Bhattacharya et al. (1992) and the GASP barometer (see text) applied to metapelite garnet assemblages, enclosing an error of ±50°C and ±1 kbar. P–T data was recalculated from mineral-chemical analyses given in Schulz and von Raumer (1993) and updated analyses. Stability fields for Ky kyanite, And andalusite, Sil sillimanite; Cd+ cordierite-in, St+ staurolite-in; St- staurolite-out and Ms- muscovite-out with univariant reaction lines are given for overall orientation in P–T coordinates after Spear (1993). **a** P–T data for Mg-rich homogenized garnet cores and retrogressive rims in mylonitic garnet gneisses. **b** P–T data from micaschists from the western series. Clinopyroxene–garnet equilibria from eclogitic amphibolite mark a high-pressure amphibolite-facies stage. **c** P–T data from micaschist series to the E. Note marked different maximal temperatures in the micaschist series (E, W). **d** Interpretative summary of P–T data and EMP monazite ages in the Col de Bérard Region of the Aiguilles Rouges Massif. The high pressure stage recorded by the eclogitic amphibolites is assigned to the Variscan P–T evolution

monazite (up to 0.06). According to the monazite–xenotime geothermometers proposed by Heinrich et al. (1997) and Pyle et al. (2001), this points to maximum formation temperatures of ~700°C for Ordovician monazites and ~600°C for the Variscan monazites. This is consistent with geothermobarometry results of garnet growth and its chemical homogenisation at high-temperatures and suggests that the homogenised garnet formed during a pre-Variscan event. Growth of pre-Variscan garnet could also explain the large spread of Y in monazite (Fig. 4a), as garnet acts as a sink with contrasting yttrium incorporation capacity at distinct temperatures (Wing et al. 2003; Pyle et al. 2001). Since Y and the REE are commonly concentrated in small accessory minerals and are little mobile in metamorphic rocks, the observed spread of Y might be also a matter of local disequilibria (Berger et al. 2005). Occurrence of polyphase monazite suggest that some of the Ordovician–Silurian monazite recrystallized during the Variscan event. It appears likely that some of the large Ordovician–Silurian monazites were replaced by pseudomorphs of allanite and apatite (Finger et al. 1998) during post-Silurian retrogression. Small monazites appearing as cluster-like satellites around apatite (Fig. 2d) then crystallized at Variscan times, interpreted as reaction structures. It appears possible that apatite was replaced by monazite through fluid-enhanced removal of Ca and F. This would be the reverse reaction of the apatite corona formation around monazite described by Finger et al. (1998) and Finger and Krenn (2007).

Variscan-age monazites are abundant in the micaschist samples with growth-zoned garnets. Their Y-contents also display a wide range. In line with the argumentation for the Ordovician–Silurian monazites, the Variscan monazites should have crystallized with and subsequent to the maximal temperatures recorded by the garnets. When the growth-zoned micaschist garnets are of Variscan age, this could explain that they were not affected by a homogenization at high temperatures. On the other hand, why are there no relics of high-temperature homogenized garnets in the micaschists? One possibility may be that the micaschist series represents a crustal section that was affected by lower pre-Variscan temperatures as the mylonitic garnet gneisses. An alternative and additional explanation could be different grain size, phase abundance and contrasting strain regimes implying reaction kinetics in mylonitic garnet gneiss and micaschists. Pre-Variscan garnet underwent decomposition and recrystallization during the Variscan pervasive shearing with formation of new foliations. In this frame the mylonitic garnet gneisses represent a special rock with a significant partition of strain. Ordovician–Silurian garnet and monazite were preserved in domains with comparably low strains while high strains were accommodated in the fine-grained mylonitic planes.

7 Comparison to the Early-Palaeozoic framework

The finding of metamorphic monazite grains of Ordovician–Silurian (~440 Ma) age and their association to high temperature homogenised garnets within a domain of a pressure-dominated Variscan metamorphism is examined within the regional geodynamic frame. In the discussion of a general model for an Ordovician active margin setting at the Gondwana margin (Cocks and Torsvik 2002; Stampfli

and Borel 2004) and the related plate-tectonic evolution (Stampfli et al. 2002; von Raumer et al. 2002), a renewed model (Stampfli et al. 2009) distinguished the evolution of the more western terranes from the more eastern terranes, the latter including the Alpine basement areas. These areas underwent an Early Ordovician evolution, also discussed as orogenic, previous to a passive margin setting, dominated by crustal extension from the Middle Ordovician at least to the Silurian (von Raumer and Stampfli 2008).

On the base of U–Pb–zircon age data from the Gotthard and Tavetsch basement areas of the External domain in the Alpine orogen, Oberli et al. (1994) and Biino (1995) found constraints for a Cambro-Ordovician magmatic-metamorphic cycle previous to the Variscan metamorphic evolution. The end of this early orogenic cycle is defined by the intrusion of the Silurian granitoids in the Gotthard area (Sergeev and Steiger 1993). Similarly, Schaltegger (1993) and Schaltegger et al. (2003) detected zircon U–Pb ages of 445 and 456 Ma for the formation of migmatites in the adjacent basement of the Aar massif. The dating of 450 Ma old gabbros in the Argentera area (Lombardo et al. 1997; Rubatto et al. 2001) and Ordovician granitoids in the Mont-Blanc area (Bussy and von Raumer 1994) provided evidence of a widespread magmatic evolution at lower crustal levels. It is recalled that also the minimum age data from meta-eclogites (Paquette et al. 1989) indicate a comparable time of intrusion of mafic volcanics.

Ordovician–Silurian events are also reported from a larger Alpine frame, as Frisch and Neubauer (1989) discussed already the main individualization of basement areas in the Austroalpine domain (e.g. Noric Terrane) for that time period. Metabasic rocks in the Graz Paleozoic (Fritz and Neubauer 1988) give evidence of a period of crustal extension, presumably in the Silurian. In the Austroalpine basement south of the Tauern an Ordovician magmatic evolution related to an active margin setting turned to an environment of extending crust during the late Ordovician and the Silurian (Schulz et al. 2004). In the Austroalpine Oetztal–Stubai basement, migmatitic leucosomes yielded an EMP monazite average age of 441 ± 18 Ma (Klötzli-Chowanetz et al. 1997; Thöny et al. 2008), indicating a Ordovician–Silurian thermal event apart from the pervasive plutonism in this region.

A polycyclic evolution had been discussed (Romer and Franz 1998; Zurbriggen et al. 1997) and confirmed (Franz and Romer 2007) in the basement of the Southern Alps. This encloses an Ordovician metamorphism prior to the regional Variscan overprint. However, a correlation of the pre-Variscan metamorphic events in the Alpine terranes to the east and the western terranes is not yet feasible: In the French Massif Central, the basement units display signs of two metamorphic cycles: Their Silurian–Early Devonian evolution, labelled also as D_1-event, is characterized by high and ultra-high pressure metamorphism which has been dated at 430–390 Ma in various parts and was followed by a Middle Devonian migmatization. During a second metamorphic cycle (D_2) at Upper Devonian to Carboniferous times and under variable lower to upper amphibolite-facies conditions, basement nappes were stacked in an inverted metamorphic pile (Faure et al. 2008; Schulz 2009).

In the Aiguilles Rouges Massif it appears likely that the Ordovician–Silurian metamorphic event was associated to the preceeding intrusions of numerous granitoids, also observed in other parts of the External domain. Judging from the thermobarometric and monazite age data (Fig. 6d) it has to remain open, whether the Ordovician–Silurian metamorphism was the direct consequence of exaggerated heat flow in an Ordovician magmatic arc setting, or if it resulted from a subsequent crustal extension.

Acknowledgments The sampling and initial studies on the Aiguilles Rouges metamorphic rocks were supported by grants from the Deutsche Forschungsgemeinschaft DFG and Schweizer Nationalfonds SNF. The electron-microprobe monazite dating required long-term analytical sessions which were facilitated by M. Göbbels, Chair of Mineralogy, Geozentrum Nordbayern at Erlangen. Technical assistance during electron-microprobe sessions at Erlangen and Technische Universität Bergakademie Freiberg/Sachsen were provided by N. Langhof, A. Richter, D. Heger and A. Renno. The English text was improved by J. Gutzmer. Thorough reviews by E. Krenn and F. Bussy and their contribution to the discussions with G. Stampfli (Lausanne) are also gratefully acknowledged.

References

Berger, A., Scherrer, N., & Bussy, F. (2005). Equilibration and disequilibration between monazite and garnet: Indication from phase composition and quantitative texture analysis. *Journal of Metamorphic Geology, 23*, 865–880.

Berman, R., Aranovich, L., & Pattison, D. (1995). Reassessment of the garnet-clinopyroxene Fe–Mg exchange thermometer: II Thermodynamic analysis. *Contributions to Mineralogy and Petrology, 115*, 30–42.

Bhattacharya, A., Mohanty, L., Maji, A., Sen, S., & Raith, M. (1992). Non-ideal mixing in the phlogopite-annite boundary: Constraint from experimental data on Fe–Mg partitioning and reformulation of the biotite-garnet geothermometer. *Contributions to Mineralogy and Petrology, 111*, 87–93.

Biino, G. (1995). Pre-Variscan evolution of the eclogitised mafic rocks from the Helvetic basement of the Central Alps. *European Journal of Mineralogy, 7*, 57–70.

Bussy, F., Hernandez, J., & von Raumer, J. (2000). Bimodal magmatism as a consequence of the post-collisonal readjustment of the thickened continental lithosphere (Aiguilles Rouges–Mont Blanc Massifs, Western Alps). *Transactions of the Royal Society of Edinburgh: Earth Sciences, 91*, 221–233.

Bussy, F., & von Raumer, J. (1994). U–Pb geochronology of Palaeozoic magmatic events in the Mont-Blanc Crystalline Massif, Western Alps. *Schweizerische Mineralogische und Petrographische Mitteilungen, 74*, 514–515.

Cocherie, A., Legendre, O., Peucat, J., & Koumelan, A. (1998). Geochronology of polygenetic monazites constrained by in situ microprobe Th–U-total lead determination: implications for lead

behaviour in monazite. *Geochimica et Cosmochimica Acta, 62*, 2475–2497.

Cocks, L., & Torsvik, T. (2002). Earth geography from 500 to 400 million years ago: a faunal and palaeomagnetic review. *Journal of the Geological Society of London, 159*, 631–644.

Dobmeier, C. (1998). Variscan P–T-deformation paths from the southwestern Aiguilles Rouges massif (External massif, Western Alps) and their implication for its tectonic evolution. *Geologische Rundschau, 87*, 107–123.

Donovan, J., Hanchar, J., Picolli, P., Schrier, M., Boatner, L., & Jarosewich, E. (2003). A re-examination of the rare-earth-element orthophosphate standards in use for electron-microprobe analysis. *Canadian Mineralogist, 41*, 221–232.

Ellis, D., & Green, D. (1979). An experimental study of the effect of Ca upon garnet-clinopyroxene Fe–Mg exchange equilibria. *Contributions to Mineralogy and Petrology, 71*, 13–22.

Faure, M., Bé Mézème, E., Cocherie, A., Rossi, P., Chemenda, A., & Boutelier, D. (2008). Devonian geodynamic evolution of the Variscan Belt, insights from the French Massif Central and Massif Armoricain. *Tectonics*, *27*, TC2005. doi:10.1029/2007TC002115.

Finger, F., Broska, I., Roberts, M., & Schermaier, A. (1998). Replacement of primary monazite by allanite–epidote coronas in an amphibolite-facies granite gneiss from the eastern Alps. *American Mineralogist, 83*, 248–258.

Finger, F., & Helmy, H. (1998). Composition and total-Pb model ages of monazite from high-grade paragneisses in the Abu Swayel area, southern Eastern Desert, Egypt. *Mineralogy and Petrology, 62*, 269–289.

Finger, F., & Krenn, E. (2007). Three metamorphic monazite generations in a high-pressure rock from the Bohemian Massif and the potentially important role of apatite in stimulating polyphase monazite growth along a P–T loop. *Lithos, 95*, 103–115.

Finger, F., Krenn, E., Riegler, G., Romano, S., & Zulauf, G. (2002). Resolving Cambrian, Carboniferous, Permian and Alpine monazite generations in the polymetamorphic basement of eastern Crete (Greece) by means of the electron microprobe. *Terra Nova, 14*, 233–240.

Fitzsimons, J., Kinny, P., Wetherley, S., & Hollingsworth, D. (2005). Bulk chemical control on metamorphic monazite growth in pelitic schists and implications for U–Pb age data. *Journal of Metamorphic Geology, 23*, 261–277.

Franz, L., & Romer, R. (2007). Caledonian high-pressure metamorphism in the Strona–Ceneri Zone (Southern Alps of southern Switzerland and northern Italy). *Swiss Journal of Geosciences, 100*, 457–467.

Frisch, W., & Neubauer, F. (1989). Pre-Alpine terranes and tectonic zoning in the Eastern Alps. In R. D. Dallmeyer (Ed.), *Terranes in the circum-Atlantic Paleozoic orogens* (Vol. 230, pp. 91–99). Geological Society of America Special Paper.

Fritz, H., & Neubauer, F. (1988). Geodynamic aspects of the Silurian and Early Devonian sedimentation in the Paleozoic of Graz (Eastern Alps). *Schweizerische Mineralogische und Petrographische Mitteilungen, 68*, 359–367.

Ganguly, J., Cheng, W., & Tirone, M. (1996). Thermodynamics of aluminosilicate garnet solid solution: New experimental data, an optimized model, and thermometric applications. *Contributions to Mineralogy and Petrology, 123*, 137–151.

Genier, F., Bussy, F., Epard, J.-L., & Baumgartner, L. (2008). Water-assisted migmatization of metagraywackes in a Variscan shear zone, Aiguilles Rouges massif, western Alps. *Lithos, 102*, 575–597.

Heinrich, W., Andrehs, G., & Franz, G. (1997). Monazite–xenotime miscibility gap thermometry I. An empirical calibration. *Journal of Metamorphic Geology, 15*, 3–16.

Holdaway, M. (2001). Recalibration of the GASP geobarometer in light of recent garnet and plagioclase activity models and versions of the garnet-biotite geothermometer. *American Mineralogist, 86*, 1117–1129.

Holland, T. (1980). The reaction albite = jadeite + quartz determined experimentally in the range 600–1200°C. *American Mineralogist, 65*, 129–134.

Holland, T., & Powell, R. (1990). An enlarged and updated internally consistent thermodynamic dataset with uncertainties and correlations: The system K_2O–Na_2O–CaO–MgO–MnO–FeO–Fe_2O_3–Al_2O_3–TiO_2–SiO_2–C–H_2–O_2. *Journal of Metamorphic Geology, 8*, 89–124.

Jarosewich, E., & Boatner, L. (1991). Rare-earth element reference samples for electron microprobe analysis. *Geostandards Newsletter, 15*, 397–399.

Klötzli-Chowanetz, E., Klötzli, U., & Koller, F. (1997). Lower Ordovician migmatisation in the Ötztal crystalline basement (Eastern Alps, Austria): Linking U–Pb and Pb–Pb dating with zircon morphology. *Schweizerische Mineralogische Petrographische Mitteilungen, 77*, 315–324.

Krenn, E., & Finger, F. (2007). Formation of monazite and rhabdophane at the expense of allanite during Alpine low temperature retrogression of metapelitic basement rocks from Crete, Greece: Microprobe data and geochronological implications. *Lithos, 95*, 130–147.

Krogh, E. (1988). The garnet–clinopyroxene Fe–Mg geothermometer: A reinterpretation of existing experimental data. *Contributions to Mineralogy and Petrology, 99*, 44–48.

Lombardo, B., Colombo, F., Compagnoni, R., Ghiglione, G., & Rubatto. D. (1997). Relics of pre-Variscan events in the Malinvern–Argentera Complex, Argentera Massif, Western Alps. In *Abstract Volume of the 3D workshop on Alpine Geological Studies. Oropa-Biella 1997* (Vol. 4, 66 p.). Milan: Quaderni de Geodinamica alpina e quaternaria.

Ludwig, K. (2001). *Users manual for Isoplot/Ex (rev. 2.49): A geochronological toolkit for Microsoft Excel* (Special Publication No. 1a, 55 p). Berkeley Geochronology Center.

Montel, J.-M., Foret, S., Veschambre, M., Nicollet, C., & Provost, A. (1996). Electron microprobe dating of monazite. *Chemical Geology, 131*, 37–51.

Newton, R. C., & Perkins, D. (1982). Thermodynamic cali-bration of geobarometers based on the assemblage garnet–plagioclase–orthopyroxene–clinopyroxene–quartz. *American Mineralogist, 67*, 203–222.

Oberli, F., Meier, M., & Biino, G. (1994). Time constraints on the pre-Variscan magmatic/metamorphic evolution of the Gotthard and Tavetsch units derived from single-zircon U–Pb results. *Schweizerische Mineralogische Petrographische Mitteilungen, 74*, 483–488.

Paquette, J., Ménot, R., & Peucat, J. (1989). REE, Sm–Nd and U–Pb zircon study of eclogites from the Alpine External massifs (Western Alps): Evidence for crustal contamination. *Earth and Planetary Sciences Letters, 96*, 181–198.

Perchuk, L. (1991). Derivation of a thermodynamically consistent set of geothermometers and barometers for metamorphic and magmatic rocks. In L. Perchuk (Ed.), *Progress in metamorphic and magmatic petrology* (pp. 93–111). Cambridge: Cambridge University Press.

Powell, R., & Holland, T. (1993). On the formulation of simple mixing models for complex phases. *American Mineralogist, 78*, 1174–1180.

Pyle, J., Spear, F., Cheney, J., & Layne, G. (2005). Monazite ages in the Chesham Pond nappe, SW New Hampshire, USA: Implications for assembly of central New England thrust sheets. *American Mineralogist, 90*, 592–606.

Pyle, J., Spear, F., Rudnick, R., & Mcdonough, W. (2001). Monazite–xenotime–garnet equilibrium in metapelites and a new monazite–garnet thermometer. *Journal of Petrology, 42*, 2083–2107.

Romer, R., & Franz, L. (1998). Ordovician Barrow-type metamorphism in the Strona–Ceneri Zone (Northern Italy) dated by U–Pb on staurolite. *Schweizerische Mineralogische Petrographische Mitteilungen, 78*, 383–395.

Rubatto, D., Schaltegger, U., Lombardo, B., Colombo, F., & Compagnoni, R. (2001). Complex Paleozoic magmatic and metamorphic evolution in the Argentera Massif (Western Alps) resolved with U–Pb dating. *Schweizerische Mineralogische Petrographische Mitteilungen, 81*, 213–228.

Schaltegger, U. (1993). The evolution of the polymetamorphic basement in the central Alps unravelled by precise U–Pb zircon dating. *Contributions to Mineralogy and Petrology, 113*, 466–478.

Schaltegger, U., Abrecht, J., & Corfu, F. (2003). The Ordovician orogeny in the Alpine basement: Constraints from geochronology and geochemistry in the Aar Massif (Central Alps). *Schweizerische Mineralogische Petrographische Mitteilungen, 83*, 183–195.

Schulz, B. (1993). P–T-deformation paths of Variscan metamorphism in the Austroalpine basement: Controls on geothermobarometry from microstructures in progressively deformed metapelites. *Schweizerische Mineralogische Petrographische Mitteilungen, 73*, 257–274.

Schulz, B. (2009). EMP-monazite age controls on P–T paths of garnet metapelites in the Variscan inverted metamorphic sequence of La Sioule, French Massif Central. *Bulletin de la Societé géologique de la France, 180*, 271–282.

Schulz, B., Bombach, K., Pawlig, S., & Brätz, H. (2004). Neoproterozoic to Early-Palaeozoic magmatic evolution in the Gondwana-derived Austroalpine basement to the south of the Tauern Window (Eastern Alps). *International Journal of Earth Sciences, 93*, 824–843.

Schulz, B., Brätz, H., Bombach, K., & Krenn, E. (2007). In situ Th–Pb dating of monazite by 266 nm laser ablation and ICP-MS with a single collector, and its control by EMP analysis. *Zeitschrift für Angewandte Geologie, 35*, 377–392.

Schulz, B., & Von Raumer, J. (1993). Syndeformational uplift of Varis-can high-pressure rocks (Col de Bérard, Aiguilles Rouges Massif, We-stern Alps). *Zeitschrift der Deutschen Geologischen Gesellschaft, 144*, 104–120.

Sergeev, S., & Steiger, R. (1993). High-precision U–Pb single zircon dating of Variscan and Caledonian magmatic cycles in the Gotthard massif, Central Swiss Alps. *Terra Nova Abstracts, 5*, 394–395.

Spear, F. (1993). *Metamorphic phase equilibra and pressure–temperature–time paths* (799 p). Mineralogical Society of America Monograph Series 1.

Spear, F., & Pyle, J. (2002). Apatite, monazite and xenotime in metamorphic rocks. In Kohn, M. et al. (Eds.), Phosphates: Geochemical, Geobiological and Materials Importance. *Reviews in Mineralogy and Geochemistry*, *48*, 293–335.

Stampfli, G., & Borel, G. (2004). The TRANSMED transects in space and time: Constraints on the paleotectonic evolution of the Mediterranean domain. In W. Cavazza, F. Roure, W. Spakman, G. M. Stampfli, & P. A. Ziegler (Eds.), *The TRANSMED Atlas: The Mediterranean Region from Crust to Mantle* (pp. 53–80). Berlin: Springer.

Stampfli, G., von Raumer, J., & Borel, G. (2002). The Paleozoic evolution of pre-Variscan terranes: from Gondwana to the Variscan collision. In: J. R. Martínez Catalán, R.D. Jr. Hatcher, R. Arenas & F. Díaz García (Eds.), *Variscan–Appalachian Dynamics: The Building of the Late Paleozoic Basement* (Vol. 364, pp. 263–280). Geological Society of America Special Paper.

Stampfli, G., von Raumer, J., Wilhem, C., & Hochard, C. (2009). Variscan terrane accretion and Gondwana-Laurussia collision, a plate-tectonic approach. *Schriftenreihe der Deutschen Gesellschaft für Geowissenschaften, 63*, 150.

St-Onge, M. (1987). Zoned poikiloblastic garnets: P–T paths and synmetamorphic uplift through 30 km of structural depth, Wopmay orogen, Canada. *Journal of Petrology, 28*, 1–21.

Suzuki, K., Adachi, M., & Kajizuka, I. (1994). Electron microprobe observations of Pb diffusion in metamorphosed detrital monazites. *Earth and Planetary Science Letters, 128*, 391–405.

Thöny, W., Tropper, P., Schennach, F., Krenn, E., Finger, F., Kaindl, R., et al. (2008). The metamorphic evolution of migmatites from the Ötztal Complex (Tyrol, Austria) and constraints on the timing of the pre-Variscan high-T event in the Eastern Alps. *Swiss Journal of Geosciences, 101*(Suppl. 1), 111–126.

Tracy, R. (1982). Compositional zoning and inclusions in metamorphic minerals. In: J. M. Ferry (Ed.), Characterization of metamorphism through mineral equilibria. *Reviews in Mineralogy*, *10*, 355–397.

Triboulet, C., & Audren, C. (1985). Continuous reactions between biotite, garnet, staurolite, kyanite-sillimanite-andalusite and P–T–time-deformation path in micaschists from the estuary of the river Vilaine, South Brittany, France. *Journal of Metamorphic Geology, 3*, 91–105.

von Raumer, J. (1969). Stilpnomelan als alpinmetamorphes Produkt im Mont-Blanc-Granit. *Contributions to Mineralogy and Petrology, 21*, 257–271.

von Raumer, J. (1998). The Palaeozoic evolution in the Alps - from Gondwana to Pangea. *Geologische Rundschau, 87*, 407–435.

von Raumer, J., Abrecht, J., Bussy, F., Lombardo, B., Ménot, R., & Schaltegger, U. (1999). The Palaeozoic metamorphic evolution of the Alpine External Massifs. *Schweizerische Mineralogische und Petrographische Mitteilungen, 79*, 5–22.

von Raumer, J., & Bussy, F. (2004). Mont-Blanc and Aiguilles-Rouges: Geology of their polymetamorphic basement (External massifs, France–Switzerland). *Mémoires de Géologie (Lausanne), 42*, 1–203.

von Raumer, J., Bussy, F., & Sharp, Z. (1996). Lac Cornu revisited: The evolution from lower to upper crust (Aiguilles-Rouges Massif, western Alps). *Schweizerische Mineralogische und Petrographische Mitteilungen, 76*, 120–121.

von Raumer, J., Bussy, F., & Stampfli, G. (2009). The Variscan evolution in the External massifs of the Alps and place in their Variscan framework. *Comptes Rendus Geoscience, 341*, 239–252.

von Raumer, J., & Neubauer, F. (1993). Late Precambrian and Palaeozoic evolution of the Alpine basement an overview. In J. F. von Raumer & F. Neubauer (Eds.), *The pre-Mesozoic geology in the Alps* (pp. 625–639). Springer: Heidelberg.

von Raumer, J., & Stampfli, G. (2008). The birth of the Rheic Ocean: Early Palaeozoic subsidence patterns and subsequent tectonic plate scenarios. *Tectonophysics, 461*, 9–20.

von Raumer, J., Stampfli, G., Borel, G., & Bussy, F. (2002). Organization of pre-Variscan basement areas at the north-Gondwanan margin. *International Journal of Earth Sciences, 91*, 35–52.

von Raumer, J., Stampfli, G., & Bussy, F. (2003). Gondwana-derived microcontinents: The constituents of the Variscan and Alpine collisional orogens. *Tectonophysics, 365*, 7–22.

Willams, M., Jercinovic, M., Goncalves, P., & Mahan, K. (2006). Format and philosophy for collecting, compiling, and reporting microprobe monazite ages. *Chemical Geology, 225*, 1–15.

Wing, B., Ferry, J., & Harrison, T. (2003). Prograde destruction and formation od monazite and allanite during contact and regional metamorphism of pelites: Petrology and geochronology. *Contributions to Mineralogy and Petrology, 145*, 228–250.

Wu, C.-M., & Cheng, B. (2006). Valid garnet-biotite (GB) geothermometry and garnet–aluminium silicate–plagioclase–quartz (GASP) geobarometry in metapelitic rocks. *Lithos, 89*, 1–23.

Zenk, M., & Schulz, B. (2004). Zoned Ca-amphiboles and related P–T evolution in metabasites from the classical Barrovian metamorphic zones in Scotland. *Mineralogical Magazine, 68*, 769–786.

Zurbriggen, R., Franz, L., & Handy, M. (1997). Pre-Variscan deformation, metamorphism and magmatism in the Strona–Ceneri Zone (southern Alps of Northern Italy and Southern Switzerland). *Schweizerische Mineralogische Petrographische Mitteilungen, 77*, 361–381.